A New Finite-Difference Time-Domain Formulation and its Equivalence with the TLM Symmetrical Condensed Node

Zhizhang Chen, *Student Member, IEEE*, Michel M. Ney, *Senior Member, IEEE*, and Wolfgang J. R. Hoefer, *Fellow, IEEE*

Abstract—**This paper describes a new finite-difference time-domain (FD-TD) formulation which is different from the FD-TD based on Yee's scheme. It is shown that the new finite-difference time-domain formulation is exactly equivalent to the symmetrical condensed node model used in the transmission line matrix (TLM) method. More specifically, the TLM method can be exactly formulated in a finite-difference form in terms of total field quantities. Due to a better field resolution and fulfillment of continuity conditions, the new FD-TD formulation or its TLM equivalent model give better convergence and accuracy than the traditional FD-TD method presently used. This is illustrated by numerical results pertaining to a finned waveguide.**

I. Introduction

RECENTLY, time domain solutions for field problems have received growing attention. Two currently employed techniques are the transmission-line matrix (TLM) method [1], [2] and the finite-difference time-domain (FD-TD) method formulated by Yee [3]. The TLM method is physical model based on Huygens' principle using interconnected transmission lines while FD-TD is an approximate discrete mathematical model directly based on Maxwell's equations. Although they have been developed independently, both methods have been extensively applied to solve similar electromagnetic field, diffusion and network problems in the time-domain [4]–[10]. The flexibility and simplicity of their basic algorithms make them very attractive. Indeed, they can treat arbitrary geometries and account for realistic features that are often neglected in theoretical analyses. Most published work on the application of these techniques has been devoted to the computation of specific structures, modelling of various types of boundaries, material parameters, implementation of graded and conformal meshes and the development of improved nodes.

Manuscript received March 28, 1991; revised August 2, 1991. This work was supported by the Telecommunication Research Institute of Ontario (TRIO) and the National Science and Engineering Council Canada (NSERC).

The authors are with the Laboratory for Electromagnetics and Microwaves, Department of Electrical Engineering, University of Ottawa, Ottawa, ON, Canada, K1N 6N5.

IEEE Log Number 9103295.

In spite of these successful applications, the exact relationship between the TLM and finite-difference formulations has been fully explained even though some work along these lines has been done by P. B. Johns [11], [12]. He demonstrated that the expanded 3D TLM node model numerically corresponds to a finite-difference scheme when they are operated in a certain way. However, there exists no FD-TD scheme that is equivalent to the symmetrical TLM condensed node, developed by Johns himself, since the six field components are not defined in the same points in Yee's finite-difference time-domain scheme. This issue is addressed in this paper where a new finite-difference time-domain formulation for Maxwell's equations is proposed and shown to be equivalent to the TLM condensed node algorithm when expressed in terms of total field quantities.

II. A New Time-Domain Finite Difference Formulation for Maxwell's Equations

A. The Two-Dimensional Case

First consider the two-dimensional Maxwell's equations for transverse magnetic (TM-to-y) waves in a stationary and sourceless medium:

$$E_x = E_z = 0, \quad H_y = 0, \tag{1}$$

$$\frac{\partial E_y}{\partial x} = -\mu \frac{\partial H_z}{\partial t}, \tag{2}$$

$$\frac{\partial E_y}{\partial z} = +\mu \frac{\partial H_x}{\partial t}, \tag{3}$$

$$\frac{\partial H_x}{\partial z} - \frac{\partial H_z}{\partial x} = +\epsilon \frac{\partial E_y}{\partial t} \tag{4}$$

where μ and ϵ are the permitivity and permeability of the medium to be modelled.

Following Yee's notation [3], we denote a Cartesian grid of points on the $x-z$ plane as

$$(i,k)=(i\delta x,k\delta z) \tag{5}$$

and any function of discrete space and time as

$$F(i\delta x,k\delta z,n\delta t)={}_nF(i,k) \tag{6}$$

where $\delta=\delta x=\delta z$ are the space discretization units (taken to be the same for simplicity), δt is the time increment, and i,k,n are integers.

Now, the 2-D region is discretized into a mesh shown in Fig. 1. Unlike in Yee's scheme [3], all the three nonzero field components of E and H are defined at a node located at the center of the 2D cell, while at the nodes on the boundary contours, only the magnetic field components tangential to the contour and the electric field normal to the mesh area are considered (Fig. 1). As a result, the E and H-field components are not separated in space but are all defined at the same grid points. This grid arrangement ensures that both the tangential E and H field components are continuous across the interface of two adjacent cells.

The finite-difference formulations at node (i,k) for (1) to (4) are therefore as follows:

$$\frac{{}_{n+\frac{1}{2}}E_y\left(i+\frac{1}{2},k\right)-{}_{n+\frac{1}{2}}E_y\left(i-\frac{1}{2},k\right)}{\delta x}=-\mu\frac{{}_{n+1}H_z(i,k)-{}_nH_z(i,k)}{\delta t} \tag{7}$$

$$\frac{{}_{n+\frac{1}{2}}E_y\left(i,k+\frac{1}{2}\right)-{}_{n+\frac{1}{2}}E_y\left(i,k-\frac{1}{2}\right)}{\delta z}=+\mu\frac{{}_{n+1}H_x(i,k)-{}_nH_x(i,k)}{\delta t} \tag{8}$$

$$\frac{{}_{n+\frac{1}{2}}H_x\left(i,k+\frac{1}{2}\right)-{}_{n+\frac{1}{2}}H_x\left(i,k-\frac{1}{2}\right)}{\delta z}-\frac{{}_{n+\frac{1}{2}}H_z\left(i+\frac{1}{2},k\right)-{}_{n+\frac{1}{2}}H_z\left(i-\frac{1}{2},k\right)}{\delta x}=+\epsilon\frac{{}_{n+1}E_y(i,k)-{}_nE_y(i,k)}{\delta t}. \tag{9}$$

From the above equation, the updated values of ${}_{n+1}E_y(i,k)$, ${}_{n+1}H_z(i,k)$ and ${}_{n+1}H_x(i,k)$ at the cell center can be obtained from the values of E and H-fields at the previous time step.

In order to get the updated values of the E and H-field components at the boundary of each cell, the energy conservation conditions, which correspond to the unitary condition of S-parameters in circuit theory, are imposed on the field quantities of each cell. That is, the field components at the boundary of each cell are decomposed into two sets of "local" plane waves (transmission line modes): one is going towards the cell center and another away from the cell center. The energy entering a cell should be equal to the energy leaving the cell at the next time step. As a result, one has:

$$\begin{aligned}&{}_{n+\frac{1}{2}}E_y\left(i,k+\frac{1}{2}\right)-Z_0\,{}_{n+\frac{1}{2}}H_x\left(i,k+\frac{1}{2}\right)\\&=2\left[{}_nE_y(i,k)-Z_0\,{}_nH_x(i,k)\right]\\&\quad-\left[{}_{n-\frac{1}{2}}E_y\left(i,k-\frac{1}{2}\right)-Z_0\,{}_{n-\frac{1}{2}}H_x\left(i,k-\frac{1}{2}\right)\right]\end{aligned} \tag{10}$$

$$\begin{aligned}&{}_{n+\frac{1}{2}}E_y\left(i,k+\frac{1}{2}\right)+Z_0\,{}_{n+\frac{1}{2}}H_x\left(i,k+\frac{1}{2}\right)\\&=2\left[{}_nE_y(i,k+1)+Z_0\,{}_nH_x(i,k+1)\right]\\&\quad-\left[{}_{n-\frac{1}{2}}E_y\left(i,k+\frac{3}{2}\right)+Z_0\,{}_{n-\frac{1}{2}}H_x\left(i,k+\frac{3}{2}\right)\right]\end{aligned} \tag{11}$$

$$\begin{aligned}&{}_{n+\frac{1}{2}}E_y\left(i+\frac{1}{2},k\right)+Z_0\,{}_{n+\frac{1}{2}}H_z\left(i+\frac{1}{2},k\right)\\&=2\left[{}_nE_y(i,k)+Z_0\,{}_nH_z(i,k)\right]\\&\quad-\left[{}_{n-\frac{1}{2}}E_y\left(i-\frac{1}{2},k\right)+Z_0\,{}_{n-\frac{1}{2}}H_z\left(i-\frac{1}{2},k\right)\right]\end{aligned} \tag{12}$$

$$\begin{aligned}&{}_{n+\frac{1}{2}}E_y\left(i+\frac{1}{2},k\right)-Z_0\,{}_{n+\frac{1}{2}}H_z\left(i+\frac{1}{2},k\right)\\&=2\left[{}_nE_y(i+1,k)-Z_0\,{}_nH_z(i+1;k)\right]\\&\quad-\left[{}_{n-\frac{1}{2}}E_y\left(i+\frac{3}{2},k\right)+Z_0\,{}_{n-\frac{1}{2}}H_z\left(i+\frac{3}{2},k\right)\right]\end{aligned} \tag{13}$$

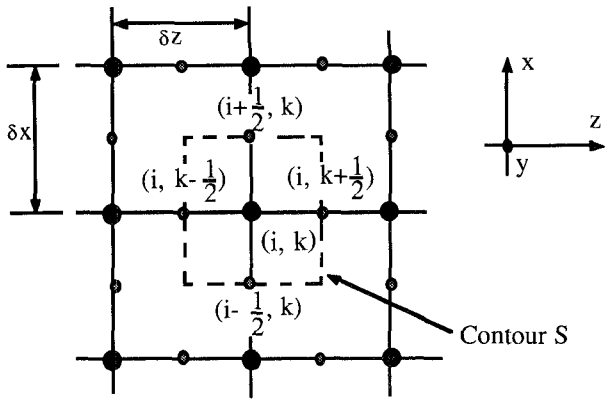

Field components defined:

For TM to -y waves:

At (i , k): Ey, Hx, Hz
At (i±½, k): Ey, Hz
At (i, k±½): Ey, Hx

Fig. 1. Grid positions for the 2D condensed TD-TD formulation.

or,

$$
\begin{aligned}
&{}_{n+\frac{1}{2}}E_y\left(i,k+\tfrac{1}{2}\right)\\
&\quad={}_nE_y(i,k)-Z_0\,{}_nH_x(i,k)\\
&\qquad+{}_nE_y(i,k+1)+Z_0\,{}_nH_x(i,k+1)\\
&\qquad-\tfrac{1}{2}\Big[{}_{n-\frac{1}{2}}E_y\left(i,k-\tfrac{1}{2}\right)-Z_0\,{}_{n-\frac{1}{2}}H_x\left(i,k-\tfrac{1}{2}\right)\\
&\qquad+{}_{n-\frac{1}{2}}E_y\left(i,k+\tfrac{3}{2}\right)+Z_0\,{}_{n-\frac{1}{2}}H_x\left(i,k+\tfrac{3}{2}\right)\Big] \qquad (14)\\
&{}_{n+\frac{1}{2}}H_x\left(i,k+\tfrac{1}{2}\right)\\
&\quad=\Big[{}_nE_y(i,k+1)+Z_0\,{}_nH_x(i,k+1)\\
&\qquad-{}_nE_y(i,k)+Z_0\,{}_nH_x(i,k)\Big]/Z_0\\
&\qquad-\tfrac{1}{2}\Big[{}_{n-\frac{1}{2}}E_y\left(i,k+\tfrac{3}{2}\right)+Z_0\,{}_{n-\frac{1}{2}}H_x\left(i,k+\tfrac{3}{2}\right)\\
&\qquad-{}_{n-\frac{1}{2}}E_y\left(i,k-\tfrac{1}{2}\right)+Z_0\,{}_{n-\frac{1}{2}}H_x\left(i,k-\tfrac{1}{2}\right)\Big]/Z_0 \qquad (15)\\
&{}_{n+\frac{1}{2}}E_y\left(i+\tfrac{1}{2},k\right)\\
&\quad={}_nE_y(i,k)+Z_0\,{}_nH_z(i,k)+{}_nE_y(i+1,k)\\
&\qquad-Z_0\,{}_nH_z(i+1,k)\\
&\qquad-\tfrac{1}{2}\Big[{}_{n-\frac{1}{2}}E_y\left(i-\tfrac{1}{2},k\right)+Z_0\,{}_{n-\frac{1}{2}}H_z\left(i-\tfrac{1}{2},k\right)\\
&\qquad-{}_{n-\frac{1}{2}}E_y\left(i+\tfrac{3}{2},k\right)-Z_0\,{}_{n-\frac{1}{2}}H_z\left(i+\tfrac{3}{2},k\right)\Big] \qquad (16)\\
&{}_{n+\frac{1}{2}}H_z\left(i+\tfrac{1}{2},k\right)\\
&\quad=\Big[{}_nE_y(i,k)+Z_0\,{}_nH_z(i,k)-{}_nE_y(i+1,k)\\
&\qquad+Z_0\,{}_nH_z(i+1,k)\Big]/Z_0\\
&\qquad-\tfrac{1}{2}\Big[{}_{n-\frac{1}{2}}E_y\left(i-\tfrac{1}{2},k\right)+Z_0\,{}_{n-\frac{1}{2}}H_z\left(i-\tfrac{1}{2},k\right)\\
&\qquad-{}_{n-\frac{1}{2}}E_y\left(i+\tfrac{3}{2},k\right)+Z_0\,{}_{n-\frac{1}{2}}H_z\left(i+\tfrac{3}{2},k\right)/Z_0 \qquad (17)
\end{aligned}
$$

where $Z_0=\sqrt{\mu/\epsilon/2}$.

B. The Three-Dimensional Case

For three-dimensional cases, Maxwell's curl equations in a stationary and sourceless medium in the time-domain are

$$\mu\frac{\partial \boldsymbol{H}}{\partial t}=-\nabla\times\boldsymbol{E}, \qquad (18)$$

$$\epsilon\frac{\partial \boldsymbol{E}}{\partial t}=\nabla\times\boldsymbol{H}. \qquad (19)$$

In a rectangular coordinate system, (18) and (19) become the following system of scalar equations:

$$\mu\frac{\partial H_x}{\partial t}=\frac{\partial E_y}{\partial z}-\frac{\partial E_z}{\partial y} \qquad (20)$$

$$\mu\frac{\partial H_y}{\partial t}=\frac{\partial E_z}{\partial x}-\frac{\partial E_x}{\partial z} \qquad (21)$$

$$\mu\frac{\partial H_z}{\partial t}=\frac{\partial E_x}{\partial y}-\frac{\partial E_y}{\partial x} \qquad (22)$$

$$\epsilon\frac{\partial E_x}{\partial t}=\frac{\partial H_z}{\partial y}-\frac{\partial H_y}{\partial z} \qquad (23)$$

$$\epsilon\frac{\partial E_y}{\partial t}=\frac{\partial H_x}{\partial z}-\frac{\partial H_z}{\partial x} \qquad (24)$$

$$\epsilon\frac{\partial E_z}{\partial t}=\frac{\partial H_y}{\partial x}-\frac{\partial H_x}{\partial y}. \qquad (25)$$

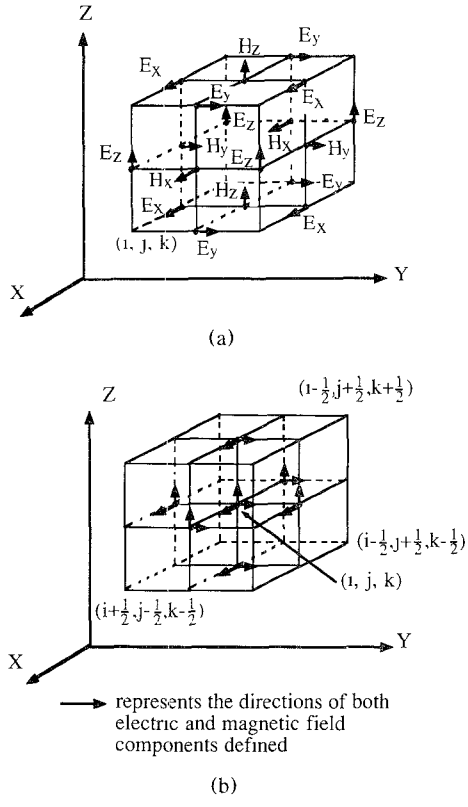

Fig. 2. (a) Positions of the field components about a unit cell of the Yee lattice. (b) Positions of the field components about 3D cell of the new finite-difference time-domain formulation.

Just like in the 2D case, we denote a Cartesian grid of points as

$$(i,j,k)=(i\delta x,j\delta y,k\delta z) \qquad (26)$$

and any function of discrete space and time as

$$F(i\delta x,j\delta y,k\delta z,n\delta t)={}_nF(i,j,k). \qquad (27)$$

$\delta=\delta x=\delta y=\delta z$ are the space discretization units (taken to be the same for simplicity), δt is the time increment, and i,j,k,n are integers.

In contrast to Yee's scheme [3] (see Fig. 2(a)), the six field components of E and H are defined at a node located at the center of the 3D cell, while at the nodes on the boundary surface of the 3D cell, only the field components tangential to the surface are considered (Fig. 2b). As in the 2D case, the E-field and H-field components are not separated in space, and both the tangential E and H field components are continuous across the interface of two adjacent cells.

By differencing (20) to (25), one can easily obtain a finite-difference formulation for Maxwell's equations.

For example, considering (23), one has

$$
\begin{aligned}
&\epsilon\frac{{}_{n+1}E_x(i,j,k)-{}_nE_x(i,j,k)}{\delta t}\\
&\quad=\frac{{}_{n+\frac{1}{2}}H_z\left(i,j+\tfrac{1}{2},k\right)-{}_{n+\frac{1}{2}}H_z\left(i,j-\tfrac{1}{2},k\right)}{\delta y}\\
&\qquad-\frac{{}_{n+\frac{1}{2}}H_y\left(i,j,k+\tfrac{1}{2}\right)-{}_{n+\frac{1}{2}}H_y\left(i,j,k-\tfrac{1}{2}\right)}{\delta z}. \qquad (28)
\end{aligned}
$$

Thus, the updated value of ${}_{n+1}E_x(i,j,k)$ at the cell center can be obtained from the values of E and H-field components at the previous time step.

The remaining finite difference equations corresponding to (20), (21), (22), (24), and (25) can be similarly constructed.

Again, in order to get updated values of both E and H on the boundary of a 3D cell, the energy conservation conditions are applied just as in the 2D situation. As a result, one has

$$\begin{aligned}{}_{n+\frac{1}{2}}E_x\left(i,j+\tfrac{1}{2},k\right)&-Z_0\,{}_{n+\frac{1}{2}}H_z\left(i,j+\tfrac{1}{2},k\right)\\&=2\left[{}_nE_x(i,j,k)-Z_0\,{}_nH_z(i,j,k)\right]\\&\quad-\left[{}_{n-\frac{1}{2}}E_x\left(i,j-\tfrac{1}{2},k\right)-Z_0\,{}_{n-\frac{1}{2}}H_z\left(i,j-\tfrac{1}{2},k\right)\right]\end{aligned}\tag{29}$$

$$\begin{aligned}{}_{n+\frac{1}{2}}E_x\left(i,j+\tfrac{1}{2},k\right)&+Z_0\,{}_{n+\frac{1}{2}}H_z\left(i,j+\tfrac{1}{2},k\right)\\&=2\left[{}_nE_x(i,j+1,k)+Z_0\,{}_nH_z(i,j+1,k)\right]\\&\quad-\left[{}_{n-\frac{1}{2}}E_x\left(i,j+\tfrac{3}{2},k\right)+Z_0\,{}_{n-\frac{1}{2}}H_z\left(i,j+\tfrac{3}{2},k\right)\right]\end{aligned}\tag{30}$$

or,

$$\begin{aligned}{}_{n+\frac{1}{2}}E_x\left(i,j+\tfrac{1}{2},k\right)&\\&={}_nE_x(i,j,k)-Z_0\,{}_nH_z(i,j,k)\\&\quad+{}_nE_x(i,j+1,k)+Z_0\,{}_nH_z(i,j+1,k)\\&\quad-\tfrac{1}{2}\left[{}_{n-\frac{1}{2}}E_x\left(i,j-\tfrac{1}{2},k\right)-Z_0\,{}_{n-\frac{1}{2}}H_z\left(i,j-\tfrac{1}{2},k\right)\right.\\&\quad\left.+{}_{n-\frac{1}{2}}E_x\left(i,j+\tfrac{3}{2},k\right)+Z_0\,{}_{n-\frac{1}{2}}H_z\left(i,j+\tfrac{3}{2},k\right)\right]\end{aligned}\tag{31}$$

$$\begin{aligned}{}_{n+\frac{1}{2}}H_z\left(i,j+\tfrac{1}{2},k\right)&\\&=\left[{}_nE_x(i,j+1,k)+Z_0\,{}_nH_z(i,j+1,k)\right.\\&\quad\left.-{}_nE_x(i,j,k)+Z_0\,{}_nH_z(i,j,k)\right]/Z_0\\&\quad-\tfrac{1}{2}\left[{}_{n-\frac{1}{2}}E_x\left(i,j+\tfrac{3}{2},k\right)+Z_0\,{}_{n-\frac{1}{2}}H_z\left(i,j+\tfrac{3}{2},k\right)\right.\\&\quad\left.-{}_{n-\frac{1}{2}}E_x\left(i,j-\tfrac{1}{2},k\right)+Z_0\,{}_{n-\frac{1}{2}}H_z\left(i,j-\tfrac{1}{2},k\right)\right]/Z_0\end{aligned}\tag{32}$$

where $Z_0=\sqrt{\mu/\epsilon}$.

The equations pertaining to updated values of other tangential E and H field components on the other boundary surfaces of a 3D cell can be constructed in a similar way or can be obtained by simply permutating subscripts (x,y,z) and coordinates (i,j,k) in the above equations.

As one can see, (7)–(17) and (28)–(32) constitute a recursive finite-difference formulation for time-dependent Maxwell's equations based on a new grid arrangement and energy conservation. When boundaries are placed half-way between two neighbouring cells, i.e. at the boundary surface of a 3D cell, the boundary conditions can be fulfilled by simply enforcing them in (10) to (12), or (29) to (30).

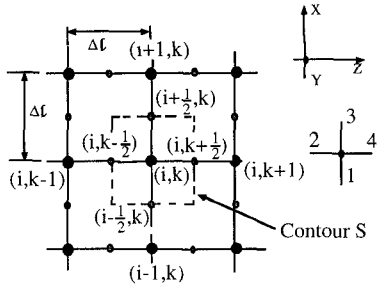

Fig. 3. 2D TLM shunt node.

Generally speaking, this finite-difference formulation ensures the continuity of both tangential electric and magnetic field components across the interfaces of cubic cells and the energy conservation within cubic cells, thus generating a stable non-dissipative solution.

It is worth mentioning that Maxwell's equations ensure, of course, the conservation of energy, but this is by no means a guarantee that a finite difference form of these equations automatically conserves energy as well, except in the infinitesimal limit. Thus energy conservation must be explicitly enforced in a FD-TD scheme to ensure it.

III. Voltage and Current Relations in the Symmetrical Condensed Node of TLM and Its Equivalence to the Finite Difference Approach

Various types of nodes have been proposed for the TLM model. For two-dimensional problems, the shunt node and the series node model [1] can be used, and for three-dimensional problems, the expanded-node [14], the asymmetrical condensed node [15] and the more recently developed symmetrical condensed node model [16] exist.

A. The 2D TLM Node

Consider a 2D TLM shunt node model [1] without inductive, capacitive and loss stubs (Fig. 3). For simplicity, suppose that each link line has the same length, $\Delta l/2$ (regular mesh), and that all the assumptions made by Johns are valid here. Note that the total voltages and currents at midpoints between two adjacent nodes are the sum or difference of the incident and reflected voltages on the link line, according to transmission line theory. For instance, if at time $(n+\frac{1}{2})\Delta t$ and position $(i,k-\frac{1}{2})$, ${}_{n+\frac{1}{2}}V_2^i(i,k-\frac{1}{2})$ is the voltage impulse going toward the node at position (i,k) and ${}_{n+\frac{1}{2}}V_2^r(i,k-\frac{1}{2})$ is the voltage impulse going away from the same node, then the total voltage at $(i,k-\frac{1}{2})$ on link line 2 is

$${}_{n+\frac{1}{2}}V_y\left(i,k-\tfrac{1}{2}\right)={}_{n+\frac{1}{2}}V_2^i\left(i,k-\tfrac{1}{2}\right)+{}_{n+\frac{1}{2}}V_2^r\left(i,k-\tfrac{1}{2}\right)\tag{33}$$

and the total current flowing in link line 2, which is along the z direction, at position $(i,k-\frac{1}{2})$ is

$${}_{n+\frac{1}{2}}I_z\left(i,k-\tfrac{1}{2}\right)=\left[{}_{n+\frac{1}{2}}V_2^i\left(i,k-\tfrac{1}{2}\right)-{}_{n+\frac{1}{2}}V_2^r\left(i,k-\tfrac{1}{2}\right)\right]/Z_0\tag{34}$$

where Z_0 is the characteristic impedance of the link line.

Note that ${}_{n+\frac{1}{2}}V_2^i(i,k-\frac{1}{2})$ arrives at the node (i,k) at time $(n+1)\Delta t$ and is denoted as ${}_{n+1}V_2^i(i,k)$, and ${}_nV_2^r(i,k)$ arrives at the midpoint $(i,k-\frac{1}{2})$ at time $(n+\frac{1}{2})\Delta t$ and is denoted as ${}_{n+\frac{1}{2}}V_2^r(i,k-\frac{1}{2})$, that is: ${}_{n+\frac{1}{2}}V_2^i(i,k-\frac{1}{2})={}_{n+1}V_2^i(i,k)$, and ${}_{n+\frac{1}{2}}V_2^r(i,k-\frac{1}{2})={}_nV_2^r(i,k)$. Then one has

$$ {}_{n+\frac{1}{2}}V\left(i,k-\tfrac{1}{2}\right)={}_{n+1}V_2^i(i,k)+{}_nV_2^r(i,k) \tag{35}$$

$$ {}_{n+\frac{1}{2}}I_z\left(i,k-\tfrac{1}{2}\right)=\left[{}_{n+1}V_2^i(i,k)-{}_nV_2^r(i,k)\right]/Z_0. \tag{36}$$

Similar voltage and current definitions and relations with their corresponding equations can be derived on the other link lines at midpoints between the nodes. Thus one obtains

$$ {}_nV_y(i,k)=\tfrac{1}{2}\left({}_nV_1^i(i,k)+{}_nV_2^i(i,k)+{}_nV_3^i(i,k)+{}_nV_4^i(i,k)\right) \tag{37}$$

$$ {}_nI_z(i,k)=\left({}_nV_4^i(i,k)-{}_nV_2^i(i,k)\right)/Z_0 \tag{38}$$

$$ {}_nI_x(i,k)=\left({}_nV_3^i(i,k)-{}_nV_1^i(i,k)\right)/Z_0 \tag{39}$$

$$ \begin{aligned} {}_{n+\frac{1}{2}}V_y\left(i+\tfrac{1}{2},k\right)&={}_{n+\frac{1}{2}}V_3^i\left(i+\tfrac{1}{2},k\right)+{}_{n+\frac{1}{2}}V_3^r\left(i+\tfrac{1}{2},k\right)\\ &={}_{n+1}V_3^i(i,k)+{}_nV_3^r(i,k) \end{aligned} \tag{40}$$

$$ \begin{aligned} {}_{n+\frac{1}{2}}V_y\left(i-\tfrac{1}{2},k\right)&={}_{n+\frac{1}{2}}V_1^i\left(i-\tfrac{1}{2},k\right)+{}_{n+\frac{1}{2}}V_1^r\left(i-\tfrac{1}{2},k\right)\\ &={}_{n+1}V_1^i(i,k)+{}_nV_1^r(i,k) \end{aligned} \tag{41}$$

$$ \begin{aligned} {}_{n+\frac{1}{2}}V_y\left(i,k+\tfrac{1}{2}\right)&={}_{n+\frac{1}{2}}V_4^i\left(i,k+\tfrac{1}{2}\right)+{}_{n+\frac{1}{2}}V_4^r\left(i,k+\tfrac{1}{2}\right)\\ &={}_{n+1}V_4^i(i,k)+{}_nV_4^r(i,k) \end{aligned} \tag{42}$$

$$ \begin{aligned} {}_{n+\frac{1}{2}}V_y\left(i,k-\tfrac{1}{2}\right)&={}_{n+\frac{1}{2}}V_2^i\left(i,k-\tfrac{1}{2}\right)+{}_{n+\frac{1}{2}}V_2^r\left(i,k-\tfrac{1}{2}\right)\\ &={}_{n+1}V_2^i(i,k)+{}_nV_2^r(i,k) \end{aligned} \tag{43}$$

$$ \begin{aligned} {}_{n+\frac{1}{2}}I_x\left(i-\tfrac{1}{2},k\right)&=\left[{}_{n+\frac{1}{2}}V_1^i\left(i-\tfrac{1}{2},k\right)-{}_{n+\frac{1}{2}}V_1^r\left(i-\tfrac{1}{2},k\right)\right]/Z_0\\ &=\left[{}_{n+1}V_1^i(i,k)-{}_nV_1^r(i,k)\right]/Z_0 \end{aligned}$$

$$ \begin{aligned} {}_{n+\frac{1}{2}}I_x\left(i+\tfrac{1}{2},k\right)&=\left[{}_{n+\frac{1}{2}}V_3^r\left(i+\tfrac{1}{2},k\right)-{}_{n+\frac{1}{2}}V_3^i\left(i+\tfrac{1}{2},k\right)\right]/Z_0\\ &=\left[{}_nV_3^i(i,k)-{}_{n+1}V_3^i(i,k)\right]/Z_0 \end{aligned} \tag{44}$$

$$ \begin{aligned} {}_{n+\frac{1}{2}}I_z\left(i,k-\tfrac{1}{2}\right)&=\left[{}_{n+\frac{1}{2}}V_2^i\left(i,k-\tfrac{1}{2}\right)-{}_{n+\frac{1}{2}}V_2^r\left(i,k-\tfrac{1}{2}\right)\right]/Z_0\\ &=\left[{}_{n+1}V_2^i(i,k)-{}_nV_2^r(i,k)\right]/Z_0 \end{aligned} \tag{45}$$

$$ \begin{aligned} {}_{n+\frac{1}{2}}I_z\left(i,k+\tfrac{1}{2}\right)&=\left[{}_{n+\frac{1}{2}}V_4^r\left(i,k+\tfrac{1}{2}\right)-{}_{n+\frac{1}{2}}V_4^i\left(i,k+\tfrac{1}{2}\right)\right]/Z_0\\ &=\left[{}_nV_4^r(i,k)-{}_{n+1}V_4^i(i,k)\right]/Z_0. \end{aligned} \tag{46}$$

In addition, the TLM impulse scattering process is defined as follows:

$$ {}_nV^r(i,k)=[S]\,{}_nV^i(i,k). \tag{47}$$

Recalling that $Z_O=\sqrt{L/C}$ and $\Delta l/\Delta t=l/\sqrt{LC}$, one can easily show from the above relations that

$$ \begin{aligned} &\frac{{}_{n+\frac{1}{2}}V_y\left(i+\frac{1}{2},k\right)-{}_{n+\frac{1}{2}}V_y\left(i-\frac{1}{2},k\right)}{\Delta l}\\ &\qquad=-L\frac{{}_{n+1}I_x(i,k)-{}_nI_x(i,k)}{\Delta t} \end{aligned} \tag{48}$$

$$ \begin{aligned} &\frac{{}_{n+\frac{1}{2}}V_y\left(i,k+\frac{1}{2}\right)-{}_{n+\frac{1}{2}}V_y\left(i,k-\frac{1}{2}\right)}{\Delta l}\\ &\qquad=-L\frac{{}_{n+1}I_z(i,k)-{}_nI_z(i,k)}{\Delta t} \end{aligned} \tag{49}$$

$$ \begin{aligned} &-\frac{{}_{n+\frac{1}{2}}I_z\left(i,k+\frac{1}{2}\right)-{}_{n+\frac{1}{2}}I_z\left(i,k-\frac{1}{2}\right)}{\Delta l}\\ &\qquad-\frac{{}_{n+\frac{1}{2}}I_x\left(i+\frac{1}{2},k\right)-{}_{n+\frac{1}{2}}I_x\left(i-\frac{1}{2},k\right)}{\Delta l}\\ &\qquad=2C\frac{{}_{n+1}V_y(i,k)-{}_nV_y(i,k)}{\Delta t} \end{aligned} \tag{50}$$

and

$$ \begin{aligned} &{}_{n+\frac{1}{2}}V_y\left(i,k+\tfrac{1}{2}\right)+Z_0\,{}_{n+\frac{1}{2}}I_z\left(i,k+\tfrac{1}{2}\right)\\ &\quad=2\left({}_nV_y(i,k)+Z_0\,{}_nI_z(i,k)\right)\\ &\qquad-\left[{}_{n-\frac{1}{2}}V_y\left(i,k-\tfrac{1}{2}\right)+Z_0\,{}_{n-\frac{1}{2}}I_z\left(i,k-\tfrac{1}{2}\right)\right] \end{aligned} \tag{51}$$

$$ \begin{aligned} &{}_{n+\frac{1}{2}}V_y\left(i,k+\tfrac{1}{2}\right)-Z_0\,{}_{n+\frac{1}{2}}I_z\left(i,k+\tfrac{1}{2}\right)\\ &\quad=2\left({}_nV_y(i,k+1)-Z_0\,{}_nI_z(i,k+1)\right)\\ &\qquad-\left[{}_{n-\frac{1}{2}}V_y\left(i,k+\tfrac{3}{2}\right)-Z_0\,{}_{n-\frac{1}{2}}I_z\left(i,k+\tfrac{3}{2}\right)\right] \end{aligned} \tag{52}$$

$$ \begin{aligned} &{}_{n+\frac{1}{2}}V_y\left(i+\tfrac{1}{2},k\right)+Z_0\,{}_{n+\frac{1}{2}}I_x\left(i+\tfrac{1}{2},k\right)\\ &\quad=2\left[{}_nV_y(i,k)+Z_0\,{}_nI_x(i,k)\right]\\ &\qquad-\left[{}_{n-\frac{1}{2}}V_y\left(i-\tfrac{1}{2},k\right)+Z_0\,{}_{n-\frac{1}{2}}I_x\left(i-\tfrac{1}{2},k\right)\right] \end{aligned} \tag{53}$$

$$ \begin{aligned} &{}_{n+\frac{1}{2}}V_y\left(i+\tfrac{1}{2},k\right)-Z_0\,{}_{n+\frac{1}{2}}I_x\left(i+\tfrac{1}{2},k\right)\\ &\quad=2\left[{}_nV_y(i+1,k)-Z_0\,{}_nI_x(i+1,k)\right]\\ &\qquad-\left[{}_{n-\frac{1}{2}}V_y\left(i+\tfrac{3}{2},k\right)-Z_0\,{}_{n-\frac{1}{2}}I_x\left(i+\tfrac{3}{2},k\right)\right] \end{aligned} \tag{54}$$

or,

$$
\begin{aligned}
&{}_{n+\frac{1}{2}}V_y\left(i,k+\tfrac{1}{2}\right)\\
&\quad={}_nV_y(i,k)+Z_0\,{}_nI_z(i,k)+{}_nV_y(i,k+1)\\
&\qquad-Z_0\,{}_nI_z(i,k+1)\\
&\qquad-\tfrac{1}{2}\left[{}_{n-\frac{1}{2}}V_y\left(i,k-\tfrac{1}{2}\right)+Z_0\,{}_{n-\frac{1}{2}}I_z\left(i,k-\tfrac{1}{2}\right)\right.\\
&\qquad\left.+{}_{n-\frac{1}{2}}V_y\left(i,k+\tfrac{3}{2}\right)-Z_0\,{}_{n-\frac{1}{2}}I_z\left(i,k+\tfrac{3}{2}\right)\right] \qquad (55)\\
&-{}_{n+\frac{1}{2}}I_z\left(i,k+\tfrac{1}{2}\right)\\
&\quad=\left[{}_nV_y(i,k+1)-Z_0\,{}_nI_z(i,k+1)\right.\\
&\qquad\left.-{}_nV_y(i,k)-Z_0\,{}_nI_z(i,k)\right]/Z_0\\
&\qquad-\tfrac{1}{2}\left[{}_{n-\frac{1}{2}}V_y\left(i,k+\tfrac{3}{2}\right)-Z_0\,{}_{n-\frac{1}{2}}I_z\left(i,k+\tfrac{3}{2}\right)\right.\\
&\qquad\left.-{}_{n-\frac{1}{2}}V_y\left(i,k-\tfrac{1}{2}\right)-Z_0\,{}_{n-\frac{1}{2}}I_z\left(i,k-\tfrac{1}{2}\right)\right]/Z_0 \qquad (56)\\
&{}_{n+\frac{1}{2}}V_y\left(i+\tfrac{1}{2},k\right)\\
&\quad={}_nV_y(i,k)+Z_0\,{}_nI_x(i,k)+{}_nV_y(i+1,k)\\
&\qquad-Z_0\,{}_nI_x(i+1,k)\\
&\qquad-\tfrac{1}{2}\left[{}_{n-\frac{1}{2}}V_y\left(i-\tfrac{1}{2},k\right)+Z_0\,{}_{n-\frac{1}{2}}I_x\left(i-\tfrac{1}{2},k\right)\right.\\
&\qquad\left.-{}_{n-\frac{1}{2}}V_y\left(i+\tfrac{3}{2},k\right)-Z_0\,{}_{n-\frac{1}{2}}I_x\left(i+\tfrac{3}{2},k\right)\right] \qquad (57)\\
&{}_{n+\frac{1}{2}}I_x\left(i+\tfrac{1}{2},k\right)\\
&\quad=\left[{}_nV_y(i,k)+Z_0\,{}_nI_x(i,k)-{}_nV_y(i+1,k)\right.\\
&\qquad\left.+Z_0\,{}_nI_x(i+1,k)\right]/Z_0\\
&\qquad+-\tfrac{1}{2}\left[{}_{n-\frac{1}{2}}V_y\left(i-\tfrac{1}{2},k\right)+Z_0\,{}_{n-\frac{1}{2}}I_x\left(i-\tfrac{1}{2},k\right)\right.\\
&\qquad\left.-{}_{n-\frac{1}{2}}V_y\left(i+\tfrac{3}{2},k\right)+Z_0\,{}_{n-\frac{1}{2}}I_x\left(i+\tfrac{3}{2},k\right)\right]/Z_0. \qquad (58)
\end{aligned}
$$

Assume that at any time and grid point, one has the following correspondences:

$$V_y \equiv E_y, \qquad (59)$$

$$I_x \equiv H_z, \qquad (60)$$

$$I_z \equiv -H_x, \qquad (61)$$

$$2C \equiv \epsilon, \qquad (62)$$

$$L \equiv \mu, \qquad (63)$$

$$\Delta l = \delta x = \delta z = \delta \qquad (64)$$

$$\Delta t = \delta t. \qquad (65)$$

By considering the above equivalences, one can easily see that (48)–(58), which were derived from the 2D TLM shunt node formulation, are exactly the same as (7) to (17) pertaining to the new finite-difference time-domain scheme for the two-dimensional case. That is, the 2D TLM shunt node model is equivalent to the FD-TD formulation.

In the case of a series node model, or if stubs are added for simulation of materials, it is not difficult to prove, by following a similar procedure, that the same conclusions can be drawn.

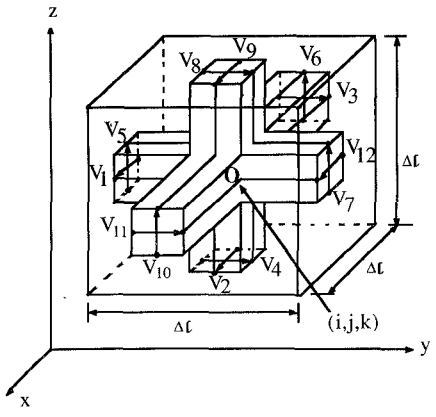

Fig. 4. 3D TLM symmetrical condensed node.

B. The 3D TLM Symmetrical Condensed Node

Consider a symmetrical condensed node without inductive, capacitive and loss stubs [16]. Each link line has the same length, $\Delta l/2$ (regular mesh) (Fig. 4). Similar to the 2D case, the total voltages and currents at midpoints between two adjacent nodes are expressed as the sum or difference of the incident and reflected voltages on the link line. For instance, the total voltage at $(i, j-\frac{1}{2}, k)$ on link line 1 is

$${}_{n+\frac{1}{2}}V_{x1}\left(i,j-\tfrac{1}{2},k\right)={}_{n+\frac{1}{2}}V_1^i\left(i,j-\tfrac{1}{2},k\right)+{}_{n+\frac{1}{2}}V_1^r\left(i,j-\tfrac{1}{2},k\right) \qquad (66)$$

and the total current flowing in link line 1, which is along the y direction, at position $(i, j-\frac{1}{2}, k)$ is

$$
\begin{aligned}
&{}_{n+\frac{1}{2}}I_{y1}\left(i,j-\tfrac{1}{2},k\right)\\
&\quad=\left[{}_{n+\frac{1}{2}}V_1^i\left(i,j-\tfrac{1}{2},k\right)-{}_{n+\frac{1}{2}}V_1^r\left(i,j-\tfrac{1}{2},k\right)\right]/Z_0 \qquad (67)
\end{aligned}
$$

where Z_0 is the characteristic impedance of the link line.

Again, as in the 2D case, ${}_{n+\frac{1}{2}}V_1^i(i,j-\frac{1}{2},k)$ arrives at the node (i,j,k) at time $(n+1)\Delta t$ and is denoted as ${}_{n+1}V_1^i(i,j,k)$, and ${}_nV_1^r(i,j,k)$ arrives at the midpoint $(i,j-\frac{1}{2},k)$ at time $(n+1)\Delta t$ and is denoted as ${}_{n+\frac{1}{2}}V_1^r(i,j-\frac{1}{2},k)$, that is, ${}_{n+\frac{1}{2}}V_1^i(i,j-\frac{1}{2},k)={}_{n+1}V_1^i(i,j,k)$, ${}_{n+\frac{1}{2}}V_1^r(i,j-\frac{1}{2},k)={}_nV_1^r(i,j,k)$. Thus,

$${}_{n+\frac{1}{2}}V_{x1}\left(i,j-\tfrac{1}{2},k\right)={}_{n+1}V_1^i(i,j,k)+{}_nV_1^r(i,j,k) \qquad (68)$$

$${}_{n+\frac{1}{2}}I_{y1}\left(i,j-\tfrac{1}{2},k\right)=\left[{}_{n+1}V_1^i(i,j,k)-{}_nV_1^r(i,j,k)\right]/Z_0. \qquad (69)$$

Therefore, one has

$$
\begin{aligned}
&{}_{n+\frac{1}{2}}V_{x12}\left(i,j+\tfrac{1}{2},k\right)\\
&\quad={}_{n+\frac{1}{2}}V^{r}_{12}\left(i,j+\tfrac{1}{2},k\right)+{}_{n+\frac{1}{2}}V^{i}_{12}\left(i,j+\tfrac{1}{2},k\right)\\
&\quad={}_{n}V^{r}_{12}(i,j,k)+{}_{n+1}V^{i}_{12}(i,j,k) \qquad (70)\\
&{}_{n+\frac{1}{2}}I_{y12}\left(i,j+\tfrac{1}{2},k\right)\\
&\quad=\left[{}_{n+\frac{1}{2}}V^{r}_{12}\left(i,j+\tfrac{1}{2},k\right)-{}_{n+\frac{1}{2}}V^{t}_{12}\left(i,j+\tfrac{1}{2},k\right)\right]/Z_0\\
&\quad=\left[{}_{n}V^{r}_{12}(i,j,k)-{}_{n+1}V^{t}_{12}(i,j,k)\right]/Z_0 \qquad (71)\\
&{}_{n+\frac{1}{2}}V_{x1}\left(i,j-\tfrac{1}{2},k\right)\\
&\quad={}_{n+\frac{1}{2}}V^{t}_{1}\left(i,j-\tfrac{1}{2},k\right)+{}_{n+\frac{1}{2}}V^{r}_{1}\left(i,j-\tfrac{1}{2},k\right)\\
&\quad={}_{n+1}V^{t}_{1}(i,j,k)+{}_{n}V^{r}_{1}(i,j,k) \qquad (72)\\
&{}_{n+\frac{1}{2}}I_{y1}\left(i,j-\tfrac{1}{2},k\right)\\
&\quad=\left[{}_{n+\frac{1}{2}}V^{t}_{1}\left(i,j-\tfrac{1}{2},k\right)-{}_{n+\frac{1}{2}}V^{r}_{1}\left(i,j-\tfrac{1}{2},k\right)\right]/Z_0\\
&\quad=\left[{}_{n+1}V^{t}_{1}(i,j,k)-{}_{n}V^{r}_{1}(i,j,k)\right]/Z_0 \qquad (73)\\
&{}_{n+\frac{1}{2}}I_{z2}\left(i,j,k-\tfrac{1}{2}\right)\\
&\quad=\left[{}_{n+\frac{1}{2}}V^{t}_{2}\left(i,j,k-\tfrac{1}{2}\right)-{}_{n+\frac{1}{2}}V^{r}_{2}\left(i,j,k-\tfrac{1}{2}\right)\right]/Z_0\\
&\quad=\left[{}_{n+1}V^{t}_{2}(i,j,k)-{}_{n}V^{r}_{2}(i,j,k)\right]/Z_0 \qquad (74)\\
&{}_{n+\frac{1}{2}}I_{z9}\left(i,j,k+\tfrac{1}{2}\right)\\
&\quad=\left[{}_{n+\frac{1}{2}}V^{r}_{9}\left(i,j,k+\tfrac{1}{2}\right)-{}_{n+\frac{1}{2}}V^{t}_{9}\left(i,j,k+\tfrac{1}{2}\right)\right]/Z_0\\
&\quad=\left[{}_{n}V^{r}_{9}(i,j,k)-{}_{n+1}V^{t}_{9}(i,j,k)\right]/Z_0. \qquad (75)
\end{aligned}
$$

In the paper presented by Johns [16], scattered voltages are related to the incident voltages through a scattering matrix $[S]$ at node (i,j,k):

$$
{}_{n}V^{r}(i,j,k)=[S]_{n}V^{i}(i,j,k) \qquad (76)
$$

with

$$
[S]=\frac{1}{2}\begin{bmatrix}
 & 1 & 1 & & & & \\
1 & & & & & & 1\\
1 & & & 1 & & & \\
 & & 1 & & 1 & & \\
 & & & 1 & & & 1\\
 & 1 & & & 1 & & \\
 & & & -1 & & & 1\\
 & & 1 & & -1 & & \\
1 & & & & & -1 & \\
 & -1 & & & 1 & & \\
-1 & & & 1 & & & \\
 & 1 & -1 & & & &
\end{bmatrix}
\begin{bmatrix}
 & 1 & & -1 & & \\
 & & -1 & & & 1\\
 & 1 & & & & -1\\
-1 & & & 1 & & \\
 & -1 & & & 1 & \\
1 & & -1 & & & \\
 & 1 & & 1 & & \\
 & 1 & & & 1 & \\
 & & 1 & & 1 & \\
1 & & 1 & & & \\
 & 1 & & & 1 & \\
 & & 1 & 1 & &
\end{bmatrix}.
$$

The voltages and circular currents at the nodes are also related to the incident voltages as follows:

$$
\begin{aligned}
{}_{n+1}V_{x}(i,j,k)&=\tfrac{2}{4}\left[{}_{n+1}V^{t}_{1}(i,j,k)+{}_{n+1}V^{t}_{2}(i,j,k)\right.\\
&\quad\left.+{}_{n+1}V^{t}_{9}(i,j,k)+{}_{n+1}V^{i}_{12}(i,j,k)\right] \qquad (77)\\
{}_{n}V_{x}(i,j,k)&=\tfrac{2}{4}\left[{}_{n}V^{i}_{1}(i,j,k)+{}_{n}V^{t}_{2}(i,j,k)\right.\\
&\quad\left.+{}_{n}V^{t}_{9}(i,j,k)+{}_{n}V^{i}_{12}(i,j,k)\right] \qquad (78)\\
{}_{n}I_{xy}(i,j,k)&=-\tfrac{1}{2}\left({}_{n}V^{t}_{1}-{}_{n}V^{t}_{3}+{}_{n}V^{t}_{11}-{}_{n}V^{t}_{12}\right)/Z_0 \qquad (79)
\end{aligned}
$$

where ${}_{n}I_{xy}(i,j,k)$ is the mesh or common current on $x-y$ plane at node (i,j,k).

Since $Z_O=\sqrt{L/C}$ and $\Delta l/\Delta t=1/\sqrt{LC}$, one can easily verify the following relations from (70) to (79):

$$
\begin{aligned}
&2C\frac{{}_{n+1}V_{x}(i,j,k)-{}_{n}V_{x}(i,j,k)}{\Delta t}\\
&\quad=-\frac{{}_{n+\frac{1}{2}}I_{y12}\left(i,j+\frac{1}{2},k\right)-{}_{n+\frac{1}{2}}I_{y1}\left(i,j-\frac{1}{2},k\right)}{\Delta l}\\
&\qquad-\frac{{}_{n+\frac{1}{2}}I_{z9}\left(i,j,k+\frac{1}{2}\right)-{}_{n+\frac{1}{2}}I_{z2}\left(i,j,k-\frac{1}{2}\right)}{\Delta l} \qquad (80)
\end{aligned}
$$

and

$$
\begin{aligned}
&{}_{n+\frac{1}{2}}V_{x12}\left(i,j+\tfrac{1}{2},k\right)+Z_{0\,n+\frac{1}{2}}I_{y12}\left(i,j+\tfrac{1}{2},k\right)\\
&\quad=2\left[{}_{n}V_{x}(i,j,k)+Z_{0\,n}I_{xy}(i,j,k)\right]\\
&\qquad-\left[{}_{n-\frac{1}{2}}V_{x1}\left(i,j-\tfrac{1}{2},k\right)+Z_{0\,n-\frac{1}{2}}I_{y1}\left(i,j-\tfrac{1}{2},k\right)\right] \qquad (81)\\
&{}_{n+\frac{1}{2}}V_{x12}\left(i,j+\tfrac{1}{2},k\right)-Z_{0\,n+\frac{1}{2}}I_{y12}\left(i,j-\tfrac{1}{2},k\right)\\
&\quad=2\left[{}_{n}V_{x}(i,j+1,k)-Z_{0\,n}I_{xy}(i,j+1,k)\right]\\
&\qquad-\left[{}_{n-\frac{1}{2}}V_{x12}\left(i,j+\tfrac{3}{2},k\right)-Z_{0\,n-\frac{1}{2}}I_{y12}\left(i,j+\tfrac{3}{2},k\right)\right] \qquad (82)
\end{aligned}
$$

or,

$$
\begin{aligned}
&{}_{n+\frac{1}{2}}V_{x12}\left(i,j+\tfrac{1}{2},k\right)\\
&\quad={}_{n}V_{x}(i,j,k)+Z_{0\,n}I_{xy}(i,j,k)+{}_{n}V_{x}(i,j+1,k)\\
&\qquad-Z_{0\,n}I_{xy}(i,j+1,k)\\
&\qquad-\tfrac{1}{2}\left[{}_{n-\frac{1}{2}}V_{x1}\left(i,j-\tfrac{1}{2},k\right)+Z_{0\,n-\frac{1}{2}}I_{y1}\left(i,j-\tfrac{1}{2},k\right)\right.\\
&\qquad\left.+{}_{n-\frac{1}{2}}V_{x12}\left(i,j+\tfrac{3}{2},k\right)-Z_{0\,n-\frac{1}{2}}I_{y12}\left(i,j+\tfrac{3}{2},k\right)\right] \qquad (83)
\end{aligned}
$$

$$
\begin{aligned}
&-{}_{n+\frac{1}{2}}I_{y12}\left(i,j+\tfrac{1}{2},k\right)\\
&\quad=\left[{}_{n}V_{x}(i,j+1,k)-Z_{0\,n}I_{xy}(i,j+1,k)-{}_{n}V_{x}(i,j,k)\right.\\
&\qquad\left.-Z_{0\,n}I_{xy}(i,j,k)\right]/Z_0\\
&\qquad-\tfrac{1}{2}\left[{}_{n-\frac{1}{2}}V_{x12}\left(i,j+\tfrac{3}{2},k\right)-Z_{0\,n-\frac{1}{2}}I_{y12}\left(i,j+\tfrac{3}{2},k\right)\right.\\
&\qquad\left.-{}_{n-\frac{1}{2}}V_{x1}\left(i,j-\tfrac{1}{2},k\right)-Z_{0\,n-\frac{1}{2}}I_{y1}\left(i,j-\tfrac{1}{2},k\right)\right]/Z_0. \qquad (84)
\end{aligned}
$$

TABLE I
THE NORMALIZED CUTOFF FREQUENCY OF THE FINNED WAVEGUIDE OBTAINED WITH THE NEW TD-FD OR TLM METHOD AND THE TD-FD ON YEE'S SCHEME

$b/\Delta\iota$	Results of New TD-FD or TLM $b/\lambda c$	Results of the TD-FD of Yee's scheme $b/\lambda c$	Result of the Transverse Resonance $b/\lambda c$	Errors compared with the Transverse Resonance (%)	
				The New TD-FD method or TLM	The TD-FD on Yee's scheme
4	0.2051	0.2050	0.2249	8.80	8.85
8	0.2155	0.2155		4.18	4.18
12	0.2189	0.2174		2.67	3.33
16	0.2206	0.2196		1.91	2.36
20	0.2217	0.2184		1.42	2.13
24	0.2224	0.2221		1.11	1.24

If one assumes that voltages and currents defined above are associated with the appropriate field components as indicated in [16]:

$$V_x \equiv E_x \text{ at } (i,j,k) \text{ and } \left(i,j\pm\tfrac{1}{2},k\right) \quad (85)$$

$$I_{xy} \equiv H_z \text{ at } (i,j,k) \quad (86)$$

$$I_z \equiv H_y \text{ at } \left(i,j,k\pm\tfrac{1}{2}\right) \quad (87)$$

$$-I_y \equiv H_z \text{ at } \left(i,j\pm\tfrac{1}{2},k\right) \quad (88)$$

$$2C \equiv \epsilon \quad (89)$$

$$\Delta l = \delta x = \delta z = \delta \quad (90)$$

$$\Delta t = \delta t \quad (91)$$

at any time step, then (80)–(84) are exactly the same as (28)–(32), one of the new finite-difference formulae for Maxwell's equations.

The remaining equations can be derived in a similar manner by assuming $V_y \equiv E_y$, $V_z \equiv E_z$, $\mu \equiv 2L$ and permutation of subscripts (x,y,z) and coordinates (i,j,k) in (86)–(88) for current and H-field components. L and C are the inductance and capacitance per unit length of the link lines. Thus, it is shown that the three-dimensional symmetrical condensed node TLM model is numerically equivalent to the finite-difference equations for Maxwell's equations. One can easily verify that the same conclusion will be reached by following a similar procedure for a condensed node with stubs.

So far it has been shown that the 2D TLM node and the 3D symmetrical condensed TLM node are each numerically equivalent to a finite-difference formulation. Furthermore, according to Johns [12], the 3D expanded node TLM model corresponds to Yee's finite-difference method. Hence, the equivalence between TLM and FD-TD formulations in general is now fully demonstrated. This suggests that any TLM algorithm can be formulated exactly in a finite-difference form and vice versa.

IV. NUMERICAL RESULTS

The new finite-difference time-domain (FD-TD) formulation (or TLM method) and Yee's finite-difference time-domain method have been compared for the two-dimensional case by computing the normalized cutoff frequency of the finned waveguide shown in Fig. 5.

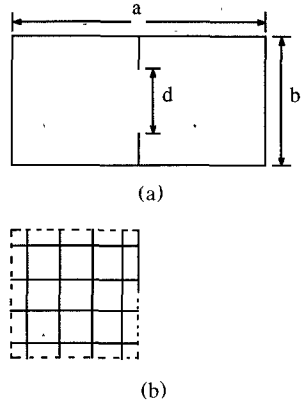

Fig. 5. (a) Crosssection of a finned rectangular waveguide. (b) Two-dimensional mesh arrangement for the waveguide shown in (a). Through introduction of symmetry conditions, only one half of the cross section is required for the analysis of the TE_{10} mode. Note the boundaries dual to those in the real structure. (– – –: magnetic wall; ——: electric wall).

Table I shows that both numerical solutions converge to the result given by transverse resonance method [17] as the number of mesh points is increased while the number of iterations remains the same in both methods. It can be seen that the new formulation has slightly better accuracy than Yee's finite-difference method, as mentioned in [18]. The reasons are that in the new model, more field components, including both tangential electric and magnetic field components at points between the cells, are computed or taken into account. Furthermore, the field components are all defined at a single location in the new formulation.

Fig. 6 shows the convergence of the numerical results with increasing number of iterations for $b/\Delta l = 4$. It can be seen that the new FD-TD formulation converges more rapidly and smoothly than Yee's FD-TD method in term of number of iterations. This is achieved at the expense of increased computational expenditure since each iteration with the new FD-TD formulation takes slightly more time. It was found that the total CPU time required for both methods was almost the same for the same required accuracy. Even in this case, the new formulation provides better field resolution due to the fact that the field components are evaluated in a larger number of positions in space. In addition, as the number of iterations in-

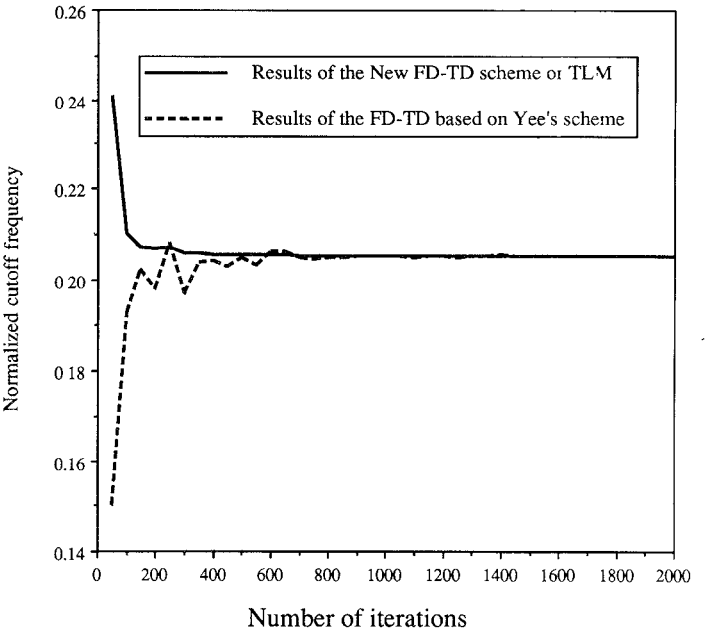

Fig. 6. Normalized cutoff frequency in the rectangular finned waveguide obtained for increasing number of iterations.

creases, the new algorithm converges very smoothly to its stable solution while Yee's scheme displays some oscillatory convergence. This can be explained by the fact mentioned earlier that in the new time-domain finite-difference formulation or the symmetrical condensed TLM node model, the continuity of the tangential field components across the interfaces of the cells and the energy conservation within the cells are ensured.

V. Conclusion

In this paper, a new finite-difference time-domain formulation for Maxwell's equation, which is different from that of Yee's scheme presently used, has been proposed. The new finite-difference equations form a kind of "condensed" model where both electric and magnetic field components are defined at the cell centers and at midpoints between adjacent cells. As a result, a better resolution and accuracy than Yee's scheme for solving electromagnetic problems are expected. This has been verified by comparing the two finite-difference formulations for the 2D cases in computing the normalized cutoff frequency of a finned waveguide. In addition, the exact equivalence between the proposed finite-difference time-domain formulation and the TLM condensed node model has been demonstrated. In other words, the TLM algorithm can be exactly formulated in finite-difference time-domain forms and vice versa. However, in spite of their equivalence, both algorithms retain their specific advantages. For instance, the finite-difference formulation has a simpler algorithm when constitutive parameters are directly introduced. On the other hand, the TLM model has certain advantages in the modelling of boundaries and the partitioning of the computational domain using Johns Matrix techniques. Further studies regarding the properties of the new FD-TD scheme in the three-dimensional case are in progress.

References

[1] P. B. Johns and R. L. Beurle, "Numerical solution of 2-dimensional scattering problems using a transmission-line matrix," *Proc. Inst. Elec. Eng.*, vol. 118, no. 9, pp. 1203–1208, Sept. 1971.

[2] P. B. Johns, "A new mathematical model to describe the physics of propagation," *The Radio and Electronic Engineer*, vol. 44, no. 12, pp. 657–666, 1974.

[3] K. S. Yee, "Numerical solution of initial boundary value problems involving Maxwell's equations," *IEEE Trans. Antennas and Propagat.*, vol. AP-14, no. 3, pp. 302–307, May 1966.

[4] A. Taflove and M. E. Brodwin, "Numerical solution of steady-state electromagnetic scattering problems using the time-dependent Maxwell's equations," *IEEE Trans. Microwave Theory Tech.*, vol. MTT-23, no. 8, pp. 623–630, Aug. 1975.

[5] A. Taflove and K. R. Umashankar, "The finite-difference time-domain (FD-TD) method for electromagnetic scattering and interaction problems," *J. Electromagnetic Waves and Applications*, vol. 1, no. 3, pp. 243–267, 1987.

[6] X. Zhang and K. Mei, "Time domain finite difference approach for the calculation of the frequency-dependent characteristic of microstrip discontinuities," *IEEE Trans. Microwave Theory Tech.*, vol. MTT-36, no. 12, pp. 1775–1787, Dec. 1987.

[7] P. B. Johns, "Application of the transmission-line matrix method to homogeneous waveguides of arbitrary cross-section," *Proc. Inst. Elec. Eng.*, vol. 119, no. 8, pp. 1086–1091, Aug. 1972.

[8] ____, "The solution of inhomogeneous waveguide problems using transmission-line matrix," *IEEE Trans. Microwave Theory Tech.*, vol. MTT-22, pp. 209–215, Mar. 1974.

[9] P. So, Eswarappa, and W. J. R. Hoefer, "A two-dimensional TLM microwave field simulator using new concepts and procedures," *IEEE Trans. Microwave Theory Tech.*, vol. 37, pp. 1877–1883, Dec. 1989.

[10] Eswarappa, G. I. Costache, and W. J. R. Hoefer, "TLM modelling of dispersive wideband absorbing boundaries with time domain diakoptics for S-parameters extraction," *IEEE Trans. Microwave Theory Tech.*, vol. MTT-41, Apr. 1990

[11] P B. Johns and G. Butler, "The consistency and accuracy of the TLM method for diffusion and its relationship to existing methods," *Int. J. Numerical Methods Eng.*, vol. 19, pp. 1549–1554, 1983.

[12] P. B. Johns, "On the relation between TLM method and finite-difference methods for Maxwell's equations," *IEEE Trans. Microwave Theory Tech.*, vol. MTT-35, no. 1, pp. 60–61, Jan. 1987.

[13] W. J. R. Hoefer, "The transmission-line matrix method-theory and application," *IEEE Trans. Microwave Theory Tech.*, vol. MTT-33, pp. 882–893, Oct. 1985.
[14] ____, "The transmission line matrix (TLM) method," *Numerical Techniques for Passive Microwave and Millimeter-Wave Structures*, T. Itoh, Ed., New York: Wiley, 1989, ch. 8, pp. 486–591
[15] P. Saguet and E. Pic, "Utilisation d'un nouveau type de noeud dans la methode TLM en 3 dimensions," *Electron. Lett.*, vol. 18, no. 11, pp. 478–480, 1982
[16] P. B. Johns, "A symmetrical condensed node for the TLM method," *IEEE Trans. Microwave Theory Tech.*, vol. MTT-35, no. 4, pp. 370–377, Apr. 1987.
[17] Y. Shih and W. J. R. Hoefer, "The accuracy of TLM analysis of finned rectangular waveguides," *IEEE Trans. Microwave Theory Tech.*, vol. MTT-28, no. 7, pp. 743–746, July 1980.
[18] D. H. Choi, "A comparison of the dispersion characteristics associated with the TLM and FD-TD methods," *International Journal of Numerical Modelling: Electronic Networks, Devices and Fields*, vol. 2, pp. 203–214, 1989.

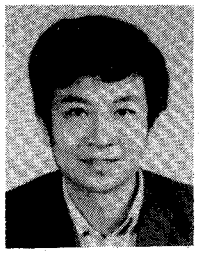

Zhizhang Chen (S'91) was born in Fujian, P. R. China, on July 3, 1962. He received the B.Eng. degree in electrical engineering from Fuzhou University, Fujian, P. R. China in 1982, and the M.Eng. degree in electrical engineering from Nanjing Institute of Technology, Nanjing, P. R. China in 1985.

From 1985 to 1988, he was employed at Fuzhou University doing research on satellite-earth direct receivers and teaching courses in the area of microwaves. Currently, he is working towards a Ph.D degree at the University of Ottawa, Ottawa, ON, Canada.

His research interests include propagation and scattering of electromagnetic waves and design of microwave devices by using numerical and analytical methods.

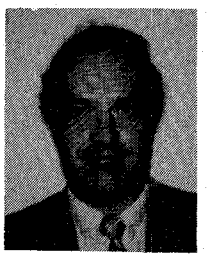

Michel M. Ney (S'80–M'82–S'83–M'83) received the Engineer Diploma from the Swiss Federal Institute of Technology of Lausanne, Switzerland, in 1976 and the Ph.D degree from the University of Ottawa, Ottawa, ON, Canada, in 1983.

Since that time he has been with the Laboratory for Electromagnetics and Microwaves of the Department of Electrical Engineering of the same institution where he is presently an Associate Professor. His research interests include passive millimeter-wave circuit design, electromagnetic engineering, electromagnetic interference and compatibility problems (EMI/C) and numerical modeling.

Dr. Ney is a Registered Professional Engineer in the province of Ontario, Canada.

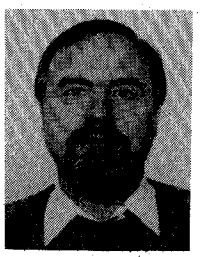

Wolfgang J. R. Hoefer (M'71–SM'78–F'91) received the diploma in electrical engineering from the Technische Hochschule Aachen, Germany, in 1965 and the D. Ing. degree from the University of Grenoble, France, in 1968.

After one year of teaching and research at the Institut Universitaire de Technologie, Grenoble, France, he joined the Department of Electrical Engineering, the University of Ottawa, Ottawa, ON, Canada, where he is currently a Professor. He spent sabbatical leaves with the Space Division of AEG-Telefunken in Backnang, Germany, the Electromagnetics Laboratory of the Institut National Polytechnique de Grenoble, France, the Space Electronics Directorate of the Communications Research Centre in Ottawa, Canada, the Universities of Rome "Tor Vergata," Italy, Sophia Antipolis, France, and München, Germany. His research interests include microwave measurement techniques, computer aided design of microwave and millimeter wave circuits, and numerical techniques for modeling electromagnetic fields.

Dr. Hoefer is a Registered Professional Engineer in the province of Ontario, Canada.